

# Alouette: Yet another encapsulated TAUOLA, but revertible

Valentin Niess<sup>a,\*</sup>

<sup>a</sup> *Université Clermont Auvergne, CNRS/IN2P3, LPC, F-63000 Clermont-Ferrand, France.*

---

## Abstract

We present an algorithm for simulating reverse Monte Carlo decays given an existing forward Monte Carlo decay engine. This algorithm is implemented in the Alouette library, a TAUOLA thin wrapper for simulating decays of  $\tau$ -leptons. We provide a detailed description of Alouette, as well as validation results.

*Keywords:* tau, decay, Monte Carlo, reverse

---

## PROGRAM SUMMARY

*Program Title:* Alouette

*CPC Library link to program files:* (to be added by Technical Editor)

*Developer's repository link:* <https://github.com/niess/alouette>

*Code Ocean capsule:* (to be added by Technical Editor)

*Licensing provisions:* LGPL-3.0

*Programming language:* C, Fortran and Python

*Nature of problem:* Perform reverse Monte Carlo decays.

*Solution method:* Invert an existing forward Monte Carlo engine using the Jacobian backward method. Apply the algorithm to  $\tau$  decays generated by TAUOLA.

## 1. Introduction

TAUOLA [1–4] is a reference Monte Carlo engine for simulating decays of  $\tau$ -leptons. It is a long standing software, initiated in the eighties, and still being contributed to nowadays (see e.g. Davidson et al. [5], Nugent et al. [6] and Chrzaszcz et al. [7]).

TAUOLA is used in the Monte Carlo simulations of many particle physics experiments. In order to motivate the present discussion, let us emphasize a particular use case. TAUOLA is also used by astroparticle experiments looking at high energy,  $E_\nu \geq 100$  GeV,  $\nu_\tau$  neutrinos. For example, neutrino telescopes like IceCube [8] or KM3NeT [9], and cosmic rays arrays like the Pierre Auger Observatory [10].

Let us briefly explain the  $\nu_\tau$  use case. The transport of  $\nu_\tau$  through the Earth is a coupled  $\nu_\tau$ - $\tau$  problem. High energy  $\nu_\tau$  undergo Deep Inelastic Scattering (DIS) collisions with nuclei, converting to  $\tau$  leptons in the Charged Current (CC) case. Since  $\tau$ -leptons are very short lived, they mostly decay in flight, thus re-producing a secondary high

---

\*Corresponding author

Email address: [niess@in2p3.fr](mailto:niess@in2p3.fr) (Valentin Niess)

Accepted for publication in Computer Physics Communications

August 18, 2022

energy  $\nu_\tau$ . This  $\nu_\tau$  regeneration scenario has been studied in details in the past (see e.g. Bugaev [11] or Bigas et al. [12]). As a result,  $\nu_\tau$  neutrinos are more penetrating than other flavours. In addition, they have specific signatures and detection methods. For example, several experiments aim at detecting Earth skimming  $\nu_\tau$ , of cosmic origin, through the radio signature of secondary  $\tau$  decaying in the atmosphere. In particular, let us refer to the GRAND collaboration [13] for additional details on this technique.

Accurate sensitivity estimates to high energy  $\tau$  from  $\nu_\tau$ , for astroparticle detectors, require sophisticated Monte Carlo computations. Various software have been developed recently in order to address this problem (see e.g. NuTauSim [14, 15], TauRunner [16], NuPropEarth [17] and Danton [18]). Of those, the most detailed Monte Carlo engines rely on TAUOLA in order to simulate  $\tau$  decays, while others use parametrisations, sometimes also derived from TAUOLA.

The efficiency of detailed sensitivity computations can be significantly improved by using reverse Monte Carlo methods, as shown by Niess and Martineau-Huynh [18] with the Danton Monte Carlo engine [19]. Reverse methods allow to sample specific final states by inverting the simulation flow. That is, by running the Monte Carlo simulation from the  $\tau$ , at the detector level, back to the primary  $\nu_\tau$ , at top of the atmosphere. However, reverse Monte Carlo should not be mistaken with time reversal. It does not time rewind the evolution of a stochastic system. Reverse Monte Carlo actually belongs to the category of Importance Sampling (IS) methods.

Reverse Monte Carlo transport engines traditionally rely on the Adjoint Monte Carlo (AMC) method [20, 21]. Recently, an alternative Backward Monte Carlo (BMC) method has been developed, differing in approach from the AMC one. BMC allows one to invert a Monte Carlo procedure, considered as a stochastic process, without the need to formulate transport equations or to compute adjoint cross-sections. Instead, Monte Carlo events are re-weighted by the Jacobian of the process, as a for a change of variable in an integral. As a particular case, the AMC process can also be used in a BMC formulation, but one is not limited to that. Let us refer to Niess et al. [22] where the BMC method is introduced in more details.

Reverse propagating  $\tau$  leptons can be done with the PUMAS [23, 24] transport engine, which implements the BMC method. Using a similar approach than PUMAS, the ENT library [25] can reverse propagate high energy neutrinos. In addition, reverting the  $\nu_\tau$ - $\tau$  transport problem requires to simulate reverse decays of  $\tau$  leptons, i.e. “undecaying” a  $\nu_\tau$  to a  $\tau$ . This is the purpose of the Alouette library, presented herein. To our knowledge, the problem of undecaying Monte Carlo particles has not been addressed previously.

This paper is separated in two parts. In the first part, i.e. section 2, we present an algorithm for undecaying particles using the BMC method and an existing forward decay engine. For the sake of clarity, the discussion specifically considers TAUOLA as forward engine. In the second part, i.e. the following sections 3 and 4, we present Alouette, a TAUOLA thin wrapper. Alouette is meant to be simple to use for  $\nu_\tau$ - $\tau$  transport problems, yet efficient and accurate. Alouette is available as a C library and as a Python package. It can operate in forward or in backward Monte Carlo mode.

## 2. Decay algorithms

### 2.1. Forward Monte Carlo

Before discussing the backward decay algorithm, let us briefly recall the forward one. TAUOLA's Monte Carlo algorithm was described in detail in several articles (see e.g. Jadach et al. [1] and references therein). Let us highlight some practical results relevant for the present discussion. A specificity of TAUOLA is that it allows one to simulate spin dependent effects in the decay of  $\tau^+\tau^-$  pairs, e.g. as produced in  $e^+e^-$  collisions. The spin states of  $\tau$  leptons are set by their production process, i.e. essentially DIS in the coupled  $\nu_\tau$ - $\tau$  transport problem. The  $\tau$  spin state is important because it significantly impacts the angular distribution of decay products.

For the purpose of  $\nu_\tau$ - $\tau$  transport, let us consider only single  $\tau$  decays herein, and let us introduce some notations. Let  $(E_0, \mathbf{p}_0)$  denote the 4-momentum of the mother  $\tau$  particle in the Laboratory frame, and let  $(E_i, \mathbf{p}_i)$  be the momenta of the daughter decay products, where  $i \geq 1$ . Note that natural units are used, where  $c = 1$ . Thus,  $E_i^2 = \mathbf{p}_i^2 + m_i^2$ , where  $m_i$  denotes the rest mass of particle  $i$ .

Let  $E_i^*$  ( $\mathbf{p}_i^*$ ) denote the energy (momentum) in the Center of Mass (CM) frame, i.e. the  $\tau$  rest frame. Thus,  $\mathbf{p}_0^* = \mathbf{0}$  and  $E_0^* = m_0$ . For the following discussion on the backward decay, it is relevant to explicitly recall the Lorentz transform from the CM frame to the Laboratory one. Let  $\beta$  be the parameter of the Lorentz transform. Then

$$E_i = \gamma (E_i^* + \beta \cdot \mathbf{p}_i^*), \quad (1)$$

$$\mathbf{p}_i = \mathbf{p}_i^* + \left( \frac{\gamma^2}{\gamma + 1} \beta \cdot \mathbf{p}_i^* + \gamma E_i^* \right) \beta, \quad (2)$$

where  $\gamma = 1/\sqrt{1 - \beta^2}$ . In the forward Monte Carlo case,  $\beta$  is determined from the mother particle properties, as  $\beta = \mathbf{p}_0/E_0$  and  $\gamma = E_0/m_0$ .

The mother's spin state is conveniently represented by a spin polarisation vector,  $\mathbf{s}^*$ , defined in the CM frame (see e.g. Jadach and Was [26]). The spin dependent part of the differential decay width can be factored as

$$d\Gamma = \sum_k (1 + \mathbf{s}^* \cdot \mathbf{h}_k^*) d\Gamma_{0,k}, \quad (3)$$

where  $d\Gamma_{0,k}$  is the spin-averaged differential decay width for the  $k^{\text{th}}$  mode. The decay polarimeter vectors,  $\mathbf{h}_k^*$ , are computed from the matrix elements of the different decay modes. Detailed results can be found in TAUOLA articles (see e.g. [1–3]). For the present purpose, it suffice to notice that the polarimeter vectors depend only on the decay products momenta  $\mathbf{p}_i^*$  in the CM frame. In particular, rotating the decay products  $\mathbf{p}_i^*$  results in an identical rotation of the polarimeter vectors  $\mathbf{h}_k^*$ . Thus, equation (3) allows one to decouple the simulation of CM polarized decays in two steps, as outlined e.g. in Jadach et al. [1]. First, an unpolarized decay is simulated in the CM frame, with corresponding polarimeter vector  $\mathbf{h}_{0,k}^*$ . By definition, this process has no preferred direction. Secondly, the actual direction of the polarimeter vector,  $\mathbf{h}_k^*$ , is randomised according to the spin factor

$$f_s = 1 + \mathbf{s}^* \cdot \mathbf{h}_k^*. \quad (4)$$

This second step determines the actual direction of decay products, which are rotated such that  $\mathbf{h}_{0,k}^*$  matches  $\mathbf{h}_k^*$ .

In practice, the direction of the polarimeter vector can be randomised using the inverse Cumulative Distribution Function (CDF) method. For this purpose, let us parametrise  $\mathbf{h}_k^*$  using spherical coordinates  $(\theta_k^*, \phi_k^*)$  with polar axis  $\mathbf{u}_z = \mathbf{s}^*/\|\mathbf{s}^*\|$ . Then, according to equation (4), the Probability Density Function (PDF) of the polar angle is

$$p(\theta_k^*) = \frac{1}{2} (1 + \alpha_k \cos(\theta_k^*)), \quad (5)$$

where  $\alpha_k = \|\mathbf{s}^*\| \|\mathbf{h}_k^*\| \in [0, 1]$ , and where the azimuthal angle  $\phi_k^*$  is uniformly distributed over  $[0, 2\pi]$ . Thus, using the inverse CDF method, the angular coordinates of the polarimeter vector are randomised as

$$\cos(\theta_k^*) = \frac{\sqrt{4\alpha_k \xi_\theta + (1 - \alpha_k)^2} - 1}{\alpha_k}, \quad (6)$$

$$\phi_k^* = 2\pi \xi_\phi, \quad (7)$$

where  $\xi_\theta$  and  $\xi_\phi$  are independent random variates uniformly distributed over  $[0, 1]$ .

The forward decay procedure is summarised below as algorithm 1. Note, that the first step, the selection of the decay mode, is optional. In practice, the user can specify a specific decay mode if desired.

---

**Algorithm 1** Forward Monte Carlo

---

- (i) Select a decay mode  $k$  with probability  $p_k = \Gamma_{0,k}/\Gamma_0$ , where  $\Gamma_0 = \sum_k \Gamma_{0,k}$ .
  - (ii) Generate a CM decay according to  $d\Gamma_{0,k}$ , i.e. assuming an unpolarized mother. Let  $\mathbf{p}_{0,i}^*$  denote the momenta of the decay products, and let  $\mathbf{h}_{0,k}^*$  be the corresponding polarimeter vector.
  - (iii) Draw the direction  $\mathbf{h}_k^*$  of the polarimeter vector according to the spin factor,  $f_s = 1 + \mathbf{s}^* \cdot \mathbf{h}_k^*$ , using equations (6) and (7).
  - (iv) Let  $R$  denote the rotation matrix from  $\mathbf{h}_{0,k}^*$  to  $\mathbf{h}_k^*$ . Rotate the momenta of decay products accordingly, as  $\mathbf{p}_i^* = R \mathbf{p}_{0,i}^*$ .
  - (v) Lorentz-transform the rotated decay products to the Laboratory frame, using equations (1) and (2), where  $\boldsymbol{\beta} = \mathbf{p}_0/E_0$ .
- 

## 2.2. Backward Monte Carlo

The backward decay problem consist in sampling the mother's particle momentum,  $\mathbf{p}_0$ , given a specific daughter one, let us say  $\mathbf{p}_j$ . This requires inverting the forward Monte Carlo decay process, i.e. algorithm 1.

### 2.2.1. Unpolarised backward decays

Let us first reduce the problem to a non ambiguous case. Let us consider a daughter particle that would be present in all decay modes, e.g. a  $\nu_\tau$  neutrino in the case of a  $\tau^-$  decay. Let us further assume that knowing the daughter particle uniquely determines

the mother's particle type, e.g. in the case of a  $\nu_\tau$  daughter the mother can only be a  $\tau^-$ , not a  $\tau^+$ .

Let us denote  $L$  the forward Monte Carlo decay process corresponding to algorithm 1, defined as

$$\mathbf{p}_j = L(\mathbf{p}_0, \mathbf{p}_j^*). \quad (8)$$

That is, the daughter (final) momentum  $\mathbf{p}_j$  is a function of the mother (initial) momentum  $\mathbf{p}_0$  and of the random variate  $\mathbf{p}_j^*$ , generated by the CM decay process. The expression of  $L$  can be derived from equation (2), substituting  $\boldsymbol{\beta} = \mathbf{p}_0/E_0$  and  $\gamma = E_0/m_0$ . For the sake of clarity, let us write the result below, as

$$L(\mathbf{p}_0, \mathbf{p}_j^*) = \mathbf{p}_j^* + \frac{1}{m_0} \left( \frac{\mathbf{p}_0 \cdot \mathbf{p}_j^*}{E_0 + m_0} + E_j^* \right) \mathbf{p}_0. \quad (9)$$

Let us further consider unpolarised decays. Then, the CM process does not depend on  $\mathbf{p}_0$ , and in particular  $\mathbf{p}_j^*$  does not. Thus, inverting equation (9) w.r.t. the first variable yields the BMC process  $L^{-1}$ , where

$$\mathbf{p}_0 = L^{-1}(\mathbf{p}_j, \mathbf{p}_j^*). \quad (10)$$

In order to perform this inversion, it is useful to notice that in the BMC case the Lorentz transform parameters can be obtained from daughter  $j$  as

$$\gamma = 1 + \frac{(\mathbf{p}_j - \mathbf{p}_j^*)^2}{E_j E_j^* + \mathbf{p}_j \cdot \mathbf{p}_j^* + m_j^2}, \quad (11)$$

$$\boldsymbol{\beta} = \frac{\gamma + 1}{\gamma(E_j + E_j^*)} (\mathbf{p}_j - \mathbf{p}_j^*). \quad (12)$$

Indeed, in the BMC case the momentum of daughter  $j$  is known both in the CM and in the Laboratory frame. Since  $\mathbf{p}_0 = \gamma m_0 \boldsymbol{\beta}$ , one obtains

$$L^{-1}(\mathbf{p}_j, \mathbf{p}_j^*) = \frac{m_0(E_j + E_j^*)}{E_j E_j^* + \mathbf{p}_j \cdot \mathbf{p}_j^* + m_j^2} (\mathbf{p}_j - \mathbf{p}_j^*). \quad (13)$$

To summarise, an unpolarised BMC process starts by generating a CM decay, as in step (i) and (ii) of algorithm 1. Thus, one gets  $\mathbf{p}_j^*$ . Since in the backward case  $\mathbf{p}_j$  is already known, one can determine the Lorentz transform parameter  $\boldsymbol{\beta}$  from equations (11) and (12). One then obtains  $\mathbf{p}_0$  from  $\mathbf{p}_0^* = \mathbf{0}$ , yielding equation (13). Thus, in practice un-polarized forward and backward Monte Carlo decays are almost identical. They differ only by the computation of  $\boldsymbol{\beta}$ .

The present case provides a clear example of the difference between reverse Monte Carlo and time reversal. The BMC process let us generate Monte Carlo decays with a fixed momentum for a specific decay product, rather than fixing the mother momentum as in forward decays. Time reverting decays would instead consist in determining the mother momentum from the momenta of all its decay products.

### 2.2.2. Polarised backward decays

In the polarised case, the decay procedure cannot be directly inverted because CM decays depend on the unknown mother's momentum  $\mathbf{p}_0$ , through the spin factor  $f_s$ . A workaround is to rely on a bias process, approximating CM decays, and then to reweight Monte Carlo events accordingly. A simple bias process would be to consider unpolarized decays. However, this can be rather inefficient when  $f_s \rightarrow 0$ , resulting in null weights. Therefore, let us instead consider the following bias distribution for the spin factor

$$f_b = 1 + \mathbf{s}_b^* \cdot \mathbf{h}_k^*, \quad (14)$$

$$\mathbf{s}_b^* = \epsilon b \frac{\mathbf{p}_j^*}{\|\mathbf{p}_j^*\|}, \quad (15)$$

where  $\epsilon = \pm 1$  depending on the  $\tau$  charge, and where  $b \in [-1, 1]$  is a configurable bias factor. Note that this is identical to the true spin factor  $f_s$ , but substituting  $\mathbf{s}^*$  with  $\mathbf{s}_b^*$ , which is known in a backward decay. With this bias process, CM decays can be randomised in the backward case using the same procedure than in the forward case, i.e. equations (6) and (7) but substituting  $\mathbf{s}^*$  with  $\mathbf{s}_b^*$ . However, a Monte Carlo weight

$$\begin{aligned} \omega_S &= f_s / f_b, \\ &= \frac{1 + \mathbf{s}^* \cdot \mathbf{h}_k^*}{1 + \mathbf{s}_b^* \cdot \mathbf{h}_k^*}, \end{aligned} \quad (16)$$

must be applied to the result in order to correct for the spin biasing. Thus, equation (13) can be used to obtain  $\mathbf{p}_0$ , as in the unpolarised case, but with  $\mathbf{p}_j^*$  generated from a bias CM process.

The rationale for using equations (14) and (15) as bias distribution is the following. High energy  $\tau$ -leptons are expected to be essentially produced with a longitudinal polarisation, left (right) handed for  $\tau^-$  ( $\tau^+$ ). In particular, this is the case for DIS (see e.g. Graczyk [27]). In addition, in the high energy limit, i.e. for  $\gamma \gg 1$ , the mother and daughter particles have similar momentum direction in the Laboratory frame. Consequently, one would typically set  $b = 1$  for decays of polarised  $\tau$ -leptons<sup>1</sup>, and  $b = 0$  otherwise.

### 2.2.3. Jacobian backward weight

Inverting the Monte Carlo process is not sufficient for a backward procedure in order to yield proper results. In addition, one must weight events by a Jacobian factor corresponding to the change of “integration variable” from  $\mathbf{p}_0$  to  $\mathbf{p}_j$ . Let us refer to section 2 of Niess et al. [22] for a detailed justification. For the present case, the backward Monte Carlo weight is computed in [Appendix A](#). Using equation (13) for  $\mathbf{p}_0 = L^{-1}(\mathbf{p}_j, \mathbf{p}_j^*)$ , one

---

<sup>1</sup>When  $b = 1$ , the denominator of equation (16) can approach zero. Then,  $\omega_S$  could tend to infinity resulting in non-convergent Monte Carlo estimates. Thus, whenever  $f_b$  is close to zero, we reject the corresponding polarimeter direction, and instead we draw a new one.

finds

$$\begin{aligned}\omega_J &= \left| \frac{\partial \mathbf{p}_0}{\partial \mathbf{p}_j} \right|, \\ &= \frac{(E_0 + E_0^*)^2 E_0}{(E_j + E_j^*)^2 E_j},\end{aligned}\tag{17}$$

where  $|\partial y/\partial x|$  denotes the determinant of the Jacobian matrix corresponding to the change of variable from  $x$  to  $y$ .

Let us emphasize an important property of BMC, not discussed previously in Niess et al. [22]. The BMC weight depends on the coordinates system used for the Monte Carlo integration. Equation (17) assumes that a Cartesian 3-momentum is used. However, this is not the case when working with a flux, e.g. like in  $\nu_\tau$ - $\tau$  transport problems. Instead, “spherical” coordinates are used, i.e. the differential flux is given per unit of momentum and of solid angle. The BMC weight in spherical coordinates,  $(p, \cos(\theta), \phi)$ , can be derived from the previous one in Cartesian coordinates,  $(p_x, p_y, p_z)$ , using Jacobians composition law. Let  $\mathbf{c}(\mathbf{s})$  denote the momentum in Cartesian (spherical) coordinates. Then

$$\left| \frac{\partial \mathbf{s}_0}{\partial \mathbf{s}_j} \right| = \left| \frac{\partial \mathbf{s}_0}{\partial \mathbf{c}_0} \right| \left| \frac{\partial \mathbf{c}_0}{\partial \mathbf{c}_j} \right| \left| \frac{\partial \mathbf{c}_j}{\partial \mathbf{s}_j} \right|,\tag{18}$$

where the middle term in equation (18) is given by equation (17). The two other terms correspond to the usual Jacobian weight for changing from Cartesian to spherical coordinates, i.e.  $|\partial \mathbf{c}/\partial \mathbf{s}| = p^2$ . Thus

$$\left| \frac{\partial \mathbf{s}_0}{\partial \mathbf{s}_j} \right| = \left| \frac{\partial \mathbf{c}_0}{\partial \mathbf{c}_j} \right| \frac{p_j^2}{p_0^2}.\tag{19}$$

Alternatively, it is frequent for transport engines to consider the kinetic energy,  $T$ , instead of the momentum. Let  $\mathbf{e} = (T, \mathbf{u})$  denote such “energy-direction” coordinates, where  $\mathbf{u}$  is a unit vector giving the momentum direction. Then, with a similar reasoning than previously one finds

$$\left| \frac{\partial \mathbf{e}_0}{\partial \mathbf{e}_j} \right| = \left| \frac{\partial \mathbf{c}_0}{\partial \mathbf{c}_j} \right| \frac{p_j E_j}{p_0 E_0}.\tag{20}$$

Note also that using the kinetic energy,  $T$ , or the total energy  $E$  as Monte Carlo variable does not modify the BMC weight, since  $T = E - m$ , thus  $|\partial T/\partial E| = 1$ .

#### 2.2.4. General backward algorithm

An additional difficulty arises when the daughter particle  $j$  can have multiple mothers, or when it is not present in all decay modes. This is the case, for example, for  $\pi$ -mesons in  $\tau$  decays. In this case, the decay mode selection procedure, i.e. step (i) in algorithm 1, must be generalised. Let  $\Gamma_{kl}$  denote the partial decay width for mother  $l$  and mode  $k$ . Let  $m_{jkl}$  be the multiplicity of particle  $j$  for the corresponding decay. In particular,  $m_{jkl} = 0$  if particle  $j$  is not a decay product for the given mode and mother. Then, the probability to select decay mode  $k$  and mother  $l$  is set to

$$p_{jkl} = \frac{m_{jkl} \Gamma_{kl}}{\sum_l \sum_k m_{jkl} \Gamma_{kl}}\tag{21}$$

In addition, when there are several daughter candidates for a given mode, i.e.  $m_{jkl} \geq 2$  e.g. as in  $\tau^- \rightarrow \pi^- \pi^- \pi^+$ , then one of them must be selected as particle  $j$ . This is done randomly with equal probabilities  $1/m_{jkl}$ . Thus, it is assumed that same type daughter particles cannot be distinguished.

Let us point out that this generalised procedure for selecting the decay mode, and the mother particle  $l$ , is again a bias procedure. Thus, as for the spin factor the biasing must be corrected by the ratio of the true selection probability,  $\Gamma_{kl}/\Gamma_l$ , to the bias one, i.e.  $p_{jkl}$ . The corresponding weight is

$$\omega_{jkl} = \frac{\sum_l \sum_k m_{jkl} \Gamma_{kl}}{m_{jkl} \Gamma_l}, \quad (22)$$

where  $\Gamma_l$  is the total decay width of mother  $l$ . Note that alternative bias selection procedures could be used in backward mode, e.g. with different probabilities. In order to be valid, the only requirement is that the bias procedure has a non null probability to select any possible mother and decay mode combination.

The general backward decay procedure is summarised below as algorithm 2. The total backward Monte Carlo weight, taking bias factors into account, is

$$\omega_B = \omega_{jkl} \omega_J \omega_S, \quad (23)$$

where  $\omega_S$ ,  $\omega_J$  and  $\omega_{jkl}$  have been given in equations (16), (17) and (22). One should also recall that the weight  $\omega_J$  actually depends on the coordinates system used for Monte Carlo variables, as discussed previously in section 2.2.3.

---

**Algorithm 2** Backward Monte Carlo

---

- (i) Select a mother  $l$  and a decay mode  $k$  with probability  $p_{jkl}$  given by equation (21).
  - (ii) Generate a CM decay according to  $d\Gamma_{0,k}$ , i.e. assuming an unpolarized mother. Let  $\mathbf{p}_{0,i}^*$  denote the momenta of the decay products, and let  $\mathbf{h}_{0,k}^*$  be the corresponding polarimeter vector.
  - (iii) Draw the direction  $\mathbf{h}_k^*$  of the polarimeter vector according to the bias factor,  $f_b = 1 + \mathbf{s}_b^* \cdot \mathbf{h}_k^*$ , using equations (6) and (7), but substituting  $\mathbf{s}^*$  with  $\mathbf{s}_b^* = b \mathbf{p}_j^* / \|\mathbf{p}_j^*\|$ .
  - (iv) Let  $R$  denote the rotation matrix from  $\mathbf{h}_{0,k}^*$  to  $\mathbf{h}_k^*$ . Rotate the momenta of decay products accordingly, as  $\mathbf{p}_i^* = R \mathbf{p}_{0,i}^*$ .
  - (v) If there are multiple candidates for the decay product  $j$ , then pick one randomly with equal probabilities.
  - (vi) Compute the Lorentz-transform parameter  $\beta$  from the daughter's momenta in the CM and Laboratory frames, using equations (11) and (12). Then, compute the mother's momentum  $\mathbf{p}_0$  using equation (2), as well as the momenta  $\mathbf{p}_{i \neq j}$  of companion decay products.
  - (vii) Request the true mother's spin polarisation,  $\mathbf{s}^*$ , from the user, given its momentum  $\mathbf{p}_0$ .
  - (viii) Compute the total backward Monte Carlo weight  $\omega_B$ , using equation (23).
-



### 3. Alouette implementation

In this section, we discuss the implementation of Alouette (version 1.0). The corresponding source is hosted on GitHub [28]. Before going into the details, let us point out that a technical overview of Alouette is provided herein. For a more practical “end-users” documentation, let us refer to Read the Docs [29]. The latter documentation contains instructions for installing Alouette, as well as a summary of the C and Python Application Programming Interfaces (APIs).

The Alouette library is structured in three layers, described in more details in the following subsections. The lowest layer is a C compliant encapsulation of the TAUOLA Fortran library. The corresponding functions and global variables are packaged with the `tauola_` prefix. This low level is internal. Its functions are not intended to be directly called by Alouette end-users. Nevertheless, it exposes some TAUOLA specific parameters that might be relevant for expert usage.

The second layer is a C library, `libalouette`, implementing the algorithms described in previous section 2 on top of TAUOLA. It contains two main functions, `alouette_decay` (forward mode) and `alouette_undecay` (backward mode), as well as some related configuration parameters.

The third layer is a Python package wrapping the C library. This layer is optional. C users would only use the second layer, i.e. `libalouette`.

#### 3.1. TAUOLA encapsulation

In this subsection we describe the low level encapsulation of TAUOLA that has been developed for Alouette. But, let us first warn the reader that some parts of this subsection are rather technical since they refer to the very details of the TAUOLA Fortran implementation. Understanding all these details is not necessary for using the 2<sup>nd</sup> and 3<sup>rd</sup> software layers of Alouette.

##### 3.1.1. TAUOLA distribution

The TAUOLA library was initially released as a Fortran package. Since then, it has been widely extended and customized. Various distributions exist today. In particular, let us point out Tauola++ from Davidson et al. [5], hosted by CERN [30]. Tauola++ is a C++ extension built over the core Fortran package.

The algorithms discussed in section 2 require an initial Monte Carlo engine performing CM decays of polarized  $\tau$ -leptons. This is done by the `DEKAY` routine implemented in TAUOLA Fortran (see e.g. Jadach et al. [1]). Since we are only concerned with single  $\tau$  decays, the C++ layer of Tauola++ is not relevant to us. However, Tauola++ also maintains and updates the Fortran source of TAUOLA, under the `tauola-fortran` directory. The latter is used as starting point for building the lower software layer of Alouette. Thus, in the following when “TAUOLA” is mentioned, it refers to the Fortran core routines shipped with Tauola++.

Namely, we use version 1.1.8 of Tauola++ tagged “for the LHC”. This release includes updated parametrisations, “new currents”, for  $\tau$  decays to 2 and 3  $\pi$ -mesons, according to Fujikawa et al. [31] and Nugent et al. [6]. However, the LHC release does not include the very latest developments, e.g. from Chrzaszcz et al. [7].

### 3.1.2. TAUOLA software design

TAUOLA is a reference Monte Carlo engine for  $\tau$  decays, producing sound physics results. However, some software design choices are unfortunate to us in order to use TAUOLA as a library in a C project. The points that we are concerned with are listed below. But, before discussing these details, let us recall that the core Fortran functionalities of TAUOLA have been designed more than 30 years ago, in a different software context than nowadays. Let us further mention that points (iv) and (v) are also discussed in Chrzaszcz et al. [7], and might be addressed by future TAUOLA developments.

- (i) TAUOLA defines hundreds of global symbols, function and structures, using Fortran 77 short names, i.e. without any library specific prefix. This complicates code readability when TAUOLA entities are used. Furthermore, it could lead to collisions with other libraries when TAUOLA is integrated in a larger framework.
- (ii) TAUOLA messages are directly written to the standard output instead of being forwarded to the library user. In addition, there is little to no severity information associated, e.g. debug, info, warning or error. This prevents integrating TAUOLA with another messaging system.
- (iii) TAUOLA errors issue a hard **STOP** statement, exiting to the OS, instead of resuming back to the caller with an error status.
- (iv) TAUOLA routines use a built-in Pseudo Random Number Generator (PRNG), **RANMAR**, shipped with the library. The PRNG is not configurable at runtime, yet partially with source pre-processing (see e.g Golonka et al. [4]). When integrating TAUOLA with another Monte Carlo, it enforces using **RANMAR** if a single PRNG is desired. Alternatively, one can use two different PRNGs, e.g. as in **Tauola++**. The latter solution can however be confusing for end-users.
- (v) TAUOLA was not written with concurrency in mind. For example, it uses common blocks and static variables that might be written concurrently in multi-threaded applications.

Solving the previous issues requires modifying TAUOLA Fortran source. Making the library thread safe would imply a significant re-writing of the source, which is beyond the present scope. However, other points can be addressed with only a little refactoring.

### 3.1.3. TAUOLA refactoring

TAUOLA source is more than 14kLOC. Modifying it manually would be tedious and error prone. Instead, modifications are done procedurally with a Python script, **wrap-tauola.py**, distributed with Alouette source. This script maps common blocks and routines, and it builds a call tree. Then, it applies the modifications discussed hereafter. Let us emphasize that these modifications are only software refactoring. They, do not change any of TAUOLA's algorithms. The resulting "refactored TAUOLA" library is packaged as a single file, **tauola.f**, also distributed with Alouette source. In addition, a companion C header file is provided, **tauola.h**, for stand-alone usage of this software layer.

First, let us recall that only the **DEKAY** routine is needed for our purpose. However, TAUOLA also exports hundreds of other sub-routines as global symbols. These sub-routines are called by **DEKAY**, but not directly by end-users. Thus, they could conveniently reside in a private scope of the library. A simple solution to this problem is to make

TAUOLA routines internal. This is achieved by relocating them into a `tauola_decay` top routine, by enclosing them with a `CONTAINS` statement. During this process, orphan routines not in the `DEKAY` call tree are removed. Similarly, the `INIMAS`, `INITDK` and `INIPHY` initialisation routines, from `tauolaFortranInterfaces/tauola_extras.f`, are also internalised. Then, only the `tauola_decay` routine needs to be exported. This top routine takes care of properly calling internal routines, for initialisation or for decay.

In addition, explicit C Application Binary Interface (ABI) names are given to external symbols, using the `BIND(C)` attribute introduced in Fortran 2003. Common blocks, as well as the user supplied `filhep` callback function, are prefixed with `tauola_`. The latter callback allows one to retrieve decay products. Note also that with this method, no compiler specific mangling occurs, e.g. C symbols have no trailing underscore.

The remaining issues (ii), (iii) and (iv), are solved by substituting `PRINT`, `STOP` and `RANMAR` statements by C callback functions, i.e. `tauola_print`, `tauola_stop` and `tauola_random`. These callbacks are implemented in the second software layer, i.e. the Alouette C library.

The `tauola_print` case deserves some more explanations. Directly substituting a callback is not possible because print formats differ between C and Fortran, and because variadic functions are not interoperable. A workaround would be to redirect Fortran prints to a buffer string, i.e. keep using Fortran formatting functions. Then, the resulting formatted string would be forwarded to the C callback function. However, this creates an extra runtime dependency on the Fortran library, e.g. `libgfortran`, because Fortran formatting functions are not part of system libraries on Unix systems. This is unfortunate, because except from this formatting issue, the compiled TAUOLA library does not depend on the Fortran library.

An alternative solution would be to forward all `PRINT` arguments to C, and then to perform the parsing of the Fortran format string, and the formatting, in C. This is however more complex, though there exist C libraries performing Fortran formatting.

Given the previous issues, and since TAUOLA is intended to be used only internally by Alouette, a simplified solution was adopted. Compound print statements, implying several formatted variables, are suppressed. We observed that those are always informative messages. Other statements must be forwarded since they might be associated to an error. However, in this case only the body text is kept without formatting. This is sufficient because the second software layer takes care of properly configuring TAUOLA and of checking input parameters to `tauola_decay`. Thus, low level TAUOLA errors seldom occur. In case a low level TAUOLA error nevertheless occurs, the unformatted error message still provides some “expert” insight on what happened.

#### 3.1.4. TAUOLA initialisation

The initialisation of TAUOLA deserves some additional explanations. First, let us point out that our refactored TAUOLA is systematically started in “new currents” mode [6, 31], i.e. by calling `INIRCHL(1)` before actually initialising TAUOLA. This is needed in order to be able to use new currents at all. However, the legacy CLEO parametrisation can be restored at any time by setting `tauola_ipcht.iver` to 0.

Secondly, TAUOLA relies on rejection sampling in order to generate Monte Carlo decays. This requires determining 20 maximum weights,  $W_{\max}$ , corresponding to the different decay modes (see e.g. Jadach et al. [1]) for more details. These weights are computed during TAUOLA’s initialisation using an opportunistic optimisation method,

i.e. by keeping the maximum out of several random trials, and by applying a 1.2 multiplicative security factor to the result. Consequently, TAUOLA’s initialisation consumes random numbers from the PRNG. In addition, although the number of trials has been set “high enough” in order to ensure a large probability of success, this method is not guaranteed to succeed.

In order to monitor the result of this initialisation step, the decay routines DADMAA, DADMEL, DADMMU, DADMKS, DADMRO and DADNEW have been slightly modified. Initially, the maximum weights value were stored in static variables WTMAX, internal to each decay routine. In the refactored TAUOLA,  $W_{\max}$  values are exported by relocating them into new common blocks, e.g. `tauola_weight_dadmaa.wtmax`, for the DADMAA decay routine. This allows one to read back their values after TAUOLA’s initialisation without interfering with any TAUOLA algorithm.

### 3.2. C library

The Alouette C library is implemented on top of the refactored TAUOLA library. Since the latter is not thread safe, the C layer was as well designed as not thread safe, which facilitates its implementation.

#### 3.2.1. Library initialisation

Alouette initialisation is automatic. It occurs on need, e.g. when calling the `alouette_decay` function. Initialisation consists mainly in calling the TAUOLA Fortran initialisation discussed previously in section 3.1.4. TAUOLA’s initialisation is performed with a dedicated (independent) instance of Alouette’s internal PRNG. Let us point out that this step does not interfere in any way with the PRNG stream exposed to Alouette end-users, since different instances are used. In addition, this dedicated PRNG stream is seeded with a fixed value in order to guarantee the success of TAUOLA’s initialisation, i.e. proper  $W_{\max}$  values. The seed has been selected as yielding median  $W_{\max}$  values for all decay modes. This is a good compromise between speed and accuracy, as further discussed in section 4.1.

At the end of TAUOLA’s initialisation, partial decay widths  $\Gamma_k$  are read back from common blocks. These data are needed for the backward Monte Carlo procedure (see e.g. equation (22)). In addition, the multiplicities  $m_{jk}$  of decays products are needed. This information is hard-coded in Alouette source. As a consequence, Alouette 1.0 is bound to a specific physics implementation of TAUOLA. That is, if decay modes are added or removed from TAUOLA, then the corresponding information must be mirrored manually in Alouette source.

Alouette initialisation can also be triggered directly with the `alouette_initialize` function. This is useful if non standard settings are needed. The latter function takes two optional parameters, as

```
enum alouette_return alouette_initialize(
    unsigned long * seed, double * xk0dec),
```

where `seed` is an alternative seed value for TAUOLA’s initialisation, and where `xk0dec` ( $k_0^{\text{decay}}$ ) specifies the soft photon cut for leptonic radiative decays (see e.g. Jezabek et al. [2]). Setting  $k_0^{\text{decay}} = 0$  disables radiative corrections for leptonic modes. Note that providing a `NULL` pointer for `seed` or for `xk0dec` results in Alouette’s default value to be used for the corresponding parameter.

### 3.2.2. Error handling

Alouette C functions indicate their execution status with an `enum alouette_return` error code. If the execution is successful, then `ALOUETTE_RETURN_SUCCESS` is returned. Otherwise, the return code indicates the type of error that occurred, as:

- `ALOUETTE_RETURN_VALUE_ERROR` e.g. for an invalid input parameter value.
- `ALOUETTE_RETURN_TAUOLA_ERROR` for a low level TAUOLA error.

The `alouette_message` function can be used in order to get a more detailed description of the last error as a characters string. The synopsis of this function is

```
const char * alouette_message(void).
```

Note that if no error occurred, then the `alouette_message` function might still return an informative or warning message generated by TAUOLA.

TAUOLA errors would normally trigger a hard `STOP`, exiting back to the OS. With the refactored TAUOLA discussed in section 3.1, these stops are however redirected to a `tauola_stop` callback function implemented in the C layer. Note that it is not possible to simply `return` from the latter callback, since this would continue TAUOLA's execution with undefined behaviour. Instead, a jump back to the calling context must be done. Thus, before any call to `tauola_decay`, a rally point is defined with `setjmp`. Then, if an error occurs, the `tauola_stop` function jumps back to the rally point using a `longjmp`.

### 3.2.3. Random stream

The Alouette library embeds a Mersenne Twister PRNG from Matsumoto and Nishimura [32]. Version MT19937 is used. The generator is exposed to users as a function pointer

```
extern float (*alouette_random)(void),
```

delivering a pseudo random `float` in  $(0, 1)$ . The `alouette_random_set` function allows one to (re)set the random stream with a given seed. Its synopsis is

```
void alouette_random_set(unsigned long * seed).
```

A `NULL` pointer can be provided as `seed` argument, in which case the seed value is drawn from the OS entropy using `/dev/urandom`. The current seed value can be retrieved using

```
unsigned long alouette_random_seed(void).
```

Let us point out that `alouette_random` is the single PRNG stream used both by TAUOLA and by Alouette. This is achieved by redirecting `RANMAR` calls, as explained previously in section 3.1. In addition, users can provide their own PRNG by overriding the `alouette_random` function pointer. Note however that in this case, Alouette's internal PRNG is still used for TAUOLA's initialisation.

### 3.2.4. Decay functions

Forward or backward Monte Carlo decays of  $\tau$ -leptons are simulated by the `alouette_decay` or `alouette_undecay` functions, respectively. These functions implement algorithms 1 and 2. Step (ii), the CM decay, is performed by the `DEKAY` function from TAUOLA's refactored interface. Other steps are done in the C layer. In addition, the

numeric output of step (ii) is checked in the C layer, for `nan` and `inf`. Indeed, in some rare cases the `DEKAY` function might return an invalid polarimeter vector, as discussed in section 3.2 of Chrzaszcz et al. [7]. Whenever this happens, the CM decay is discarded and a new one is simulated.

The decay function has the following synopsis

```
enum alouette_return alouette_decay(
    int mode, int pid, const double momentum[3],
    const double * polarisation,
    struct alouette_products * products).
```

It takes as input the mother Particle Identifier (PID), according to the Particle Data Group [33] (PDG), as well as the mother 3-momentum. Decay products are stored in a `struct alouette_products`. This is a dedicated storage structure using fixed size arrays. The structure is tailored for up to 7 decay products, the maximum possible according to TAUOLA (see e.g. table 1). It is defined as

```
struct alouette_products {
    int size, pid[7];
    double P[7][4], polarimeter[3], weight;
}.
```

The actual number of decay products is encoded in the `size` field. Other fields record the PID and 4-momenta of decay products. The `weight` field is not used in the forward Monte Carlo case. For consistency with the backward case it is set to 1.

Let us point out that the `alouette_products` structure is not intended for massively storing generic Monte Carlo data. Using a fixed size is not optimal for that purpose. However, it is efficient as a temporary (volatile) format, since the number of decay products is not known a priori when calling `alouette_decay`.

As in TAUOLA, one can also enforce a specific decay mode when calling an Alouette decay function. The decay mode is indicated as an integer number, where “0” stands for all modes. The TAUOLA version wrapped by Alouette 1.0 (i.e. Tauola++ 1.1.8 for LHC) considers 22 decay modes<sup>2</sup>, described in table 1. Some decay modes are composite. They proceed through resonances, e.g.  $\tau^- \rightarrow a_1^- \nu_\tau$ , or they result in  $K^0$  particles rendered by TAUOLA as  $K_S$  or as  $K_L$ . In these cases, the decay products vary randomly for a given mode, which is problematic for the backward procedure described in section 2. Therefore, a normalisation procedure is applied, as following.

Whenever a decay mode can lead to different decay products, Alouette defines sub-modes for each case. These sub-modes are indexed as  $i = 100m + s$ , where  $m$  is TAUOLA’s mode index and  $s$  the sub-mode index. For example, for the 5<sup>th</sup> mode,  $\tau^- \rightarrow a_1^- \nu_\tau$ , two sub-modes are simulated by TAUOLA,  $a_1 \rightarrow \pi^+ \pi^- \pi^- \nu_\tau$  and  $a_1 \rightarrow \pi^0 \pi^0 \pi^- \nu_\tau$ , which are respectively indexed as 501 and 502 by Alouette. The relative branching ratios of sub-modes are encoded in TAUOLA common blocks, e.g. `tauola_taukle.bra1` for  $a_1$ . This allows one to compute the total branching ratio of a given sub-mode. Then, in step (i) of algorithm 2, composite decay modes are replaced by their sub-modes. In addition, one needs to enforce a specific sub-mode of decay in step (ii) whenever it is selected. This

---

<sup>2</sup>In comparison, TAUOLA version from Chrzaszcz et al. [7] provides 196 decays modes.

Table 1:  $\tau^-$  decay modes and sub-modes available in Alouette 1.0. Composite modes are labelled with a \*, and their sub-modes are indicated underneath. Note that leptonic modes, indexed 1 and 2, might radiate an additional  $\gamma$ .

| Index | Products                                | Index | Products                         |
|-------|---|-------|----------------------------------|
| 1     | $\nu_\tau \bar{\nu}_e e^- (\gamma)$     | 14    | $\nu_\tau \pi^- K^- K^+$         |
| 2     | $\nu_\tau \bar{\nu}_\mu \mu^- (\gamma)$ | 15*   | $\nu_\tau \pi^- K^0 \bar{K}^0$   |
| 3     | $\nu_\tau \pi^-$                        | 1501  | $\nu_\tau \pi^- 2K_S$            |
| 4     | $\nu_\tau \pi^- \pi^0$                  | 1502  | $\nu_\tau \pi^- K_S K_L$         |
| 5*    | $\nu_\tau a_1^-$                        | 1503  | $\nu_\tau \pi^- 2K_L$            |
| 501   | $\nu_\tau 2\pi^- \pi^+$                 | 16*   | $\nu_\tau \pi^0 K^0 K^-$         |
| 502   | $\nu_\tau \pi^- 2\pi^0$                 | 1601  | $\nu_\tau \pi^0 K_S K^-$         |
| 6     | $\nu_\tau K^-$                          | 1602  | $\nu_\tau \pi^0 K_L K^-$         |
| 7*    | $\nu_\tau K^{*-}$                       | 17    | $\nu_\tau 2\pi^0 K^-$            |
| 701   | $\nu_\tau \pi^- K_S$                    | 18    | $\nu_\tau \pi^- \pi^+ K^-$       |
| 702   | $\nu_\tau \pi^- K_L$                    | 19*   | $\nu_\tau \pi^- \pi^0 \bar{K}^0$ |
| 703   | $\nu_\tau \pi^0 K^-$                    | 1901  | $\nu_\tau \pi^- \pi^0 K_S$       |
| 8     | $\nu_\tau 2\pi^- \pi^0 \pi^+$           | 1902  | $\nu_\tau \pi^- \pi^0 K_L$       |
| 9     | $\nu_\tau \pi^- 3\pi^0$                 | 20    | $\nu_\tau \pi^- \pi^0 \eta$      |
| 10    | $\nu_\tau 2\pi^- 2\pi^0 \pi^+$          | 21    | $\nu_\tau \pi^- \pi^0 \gamma$    |
| 11    | $\nu_\tau 3\pi^- 2\pi^+$                | 22*   | $\nu_\tau K^- K^0$               |
| 12    | $\nu_\tau 3\pi^- \pi^0 2\pi^+$          | 2201  | $\nu_\tau K^- K_S$               |
| 13    | $\nu_\tau 2\pi^- 3\pi^0 \pi^+$          | 2202  | $\nu_\tau K^- K_L$               |

is achieved by temporarily overriding TAUOLA relative branching ratios for sub modes, e.g. setting `tauola_taukle.bra1 = 1` enforces simulating mode 501. Note that this is a proper (intended) usage of TAUOLA, as described in section 6 of Jadach et al. [3].

Let us point out that due to radiative corrections, the leptonic decay modes, indexed as 1 and 2, are still composite. The decay products might contain an extra  $\gamma$ , or not. In this case, it is not possible to explicitly select between both sub-modes. As a result, Alouette cannot backward decay  $\gamma$  particles to  $\tau$ -leptons.

The interface of the undecay function is similar to the decay one. Its synopsis is

```
enum alouette_return alouette_undecay(
    int mode, int pid, const double momentum[3],
    alouette_polarisation_cb * polarisation,
    struct alouette_products * products),
```

where the `pid` and `momentum` arguments correspond to the daughter particle, not to the mother one. The BMC weight, given by equation (23), is filled to the `weight` field of the `alouette_products` structure.

In forward mode, the mother's spin polarisation is specified directly as a 3-vector. In backward mode, this would not be convenient since the latter might depend on the mother momentum, which is only returned at output of the undecay function. Thus, the spin polarisation is instead provided by a callback function in backward mode, defined as

```
typedef void alouette_polarisation_cb(
    int pid, const double momentum[3],
    double * polarisation)
```

where `pid` and `momentum` are given for the mother particle in this case. This method allows one to query the polarisation value during the course of the backward simulation.

The undecay function has three additional configurable parameters, defined as global variables. The `int alouette_undecay_mother` variable allows one to set a specific mother particle in backward decays, by indicating its PID as an integer. Setting this variable to zero, which is the default behaviour, results in both  $\tau^-$  and  $\tau^+$  to be considered as mother candidate.

The `double alouette_undecay_bias` variable allows one to set the value of the bias, parameter  $b$  in equation (15). It defaults to 1, i.e. longitudinally polarized  $\tau$ -leptons, which should be relevant for high energy applications. In other use cases, setting a lower value might be more efficient.

The `alouette_undecay_scheme` variable allows one to specify the Monte Carlo integration variables when computing the BMC weight, as an `enum alouette_undecay_scheme` value. The default is to assume a Cartesian 3-momentum, which is consistent with Alouette and TAUOLA APIs. But, the two alternative schemes discussed in section 2.2.3 are available as well, i.e. spherical coordinates for the 3-momentum or an energy-direction representation. In particular, if Alouette is chained with PUMAS [23, 24] for a BMC simulation, then the energy-direction scheme must be selected in order to be consistent with PUMAS.



### 3.3. Python package

#### 3.3.1. Package implementation

The `alouette` Python 3 package is a wrapper of the C library, `libalouette`, built using `ffi` [34] and `numpy` [35]. As a result, the Python and C APIs of Alouette are very similar. The `ffi` package is used in API mode in order to generate Python bindings for `libalouette`. The buffer protocol allows one to expose numeric C data as `numpy.ndarray`. By combining both `ffi` and `numpy`, the Python implementation of Alouette is straightforward, only requiring some wrapping. In particular, the `@property` decorator of Python class instances is convenient for wrapping low level C / Fortran data as attributes. Since this decorator is not available for base Python objects, but only for class instances, we make intensive use of singleton classes.

The `alouette_initialise` and `alouette_decay` C functions are wrapped as `alouette.initialise` and `alouette.decay` Python functions. Decay products are wrapped as `alouette.Products` class. This class exposes C data, e.g. PIDs or momenta, as read-only `numpy` arrays.

The `alouette_undecay` function is implemented as an `alouette.undecay` singleton class. This lets it operate as a function but with managed properties. Thus, calling `alouette.undecay(...)` performs a backward Monte Carlo decay. But, in addition `undecay` has three attributes, `undecay.mother`, `undecay.bias` and `undecay.scheme`, which allows one to manipulate the corresponding C global variables.

Using a similar approach, Alouette’s random stream is wrapped by an `alouette.random` singleton class. Calling `alouette.random()` returns the next pseudo-random number from the stream. The `random.seed` field exposes the current seed as a read only attribute. The stream can be (re)set with the `random.set(seed=None)` function. If no explicit seed is provided, then a `NULL` pointer is passed to `alouette_random_set`, i.e. the random seed is drawn from the OS entropy using `/dev/urandom`.

In addition, some relevant TAUOLA common blocks are exposed, in `alouette.tauola` submodule, using singleton classes. E.g., the parametrisation version for decays to 2 and 3 pions can be read and modified as `tauola.ipcht.iver`.

#### 3.3.2. Package distribution

The Python Packaging Index (PyPI) and its associated package manager, `pip`, are used for distributing Alouette. Binary distributions, based on the “wheel” format, have become prevalent on PyPI, over source distributions. Binary distributions are convenient for end-users, since the software is already compiled. However, building a portable binary distribution implies additional technical complications for developers, not discussed herein.

Binary distributions of Alouette are generated using GitHub’s Continuous Integration (CI) workflow. They are available from PyPI [36] as Python wheels for Linux and for OSX. Alouette wheels have ABI compatibility with system libraries down to `glibc` 2.5, on Linux, or down to OSX 10.9. Let us emphasize that the wheels contain a binary of `libalouette`, that can be used independently of the Python package. In addition, the wheels are shipped with a small executable script, `alouette-config`, providing C compilation flags for Alouette.

## 4. Alouette validation

Various validation tests of Alouette have been carried out. In the following we present some of the final results obtained with the Python alouette package, using v1.0.1 of Alouette. Intermediary tests have been performed as well, not detailed below. In particular, the C library has been checked to be error free according to valgrind [37]. Floating point errors have also been tracked down by enabling floating point exceptions, using `fenv.h`. In addition, the Python API is unit tested with a 100 % coverage. This is done on each source update, using GitHub’s CI workflow. Similar, but more informal tests have also been carried out for the C API.

### 4.1. Initialisation

A preliminary concern is to check that TAUOLA is properly initialised by Alouette. Indeed, let us recall that TAUOLA’s initialisation, and thus its subsequent physics results, depend on the seed value provided to Alouette’s internal PRNG. The seed value determines a set of 20 estimates of maximum weights,  $W_{\max}$ . These maximum weights are used by TAUOLA in order to simulate the kinematics of decays by rejections sampling, as discussed previously in section 3.1.4. In the following, let us write  $W_{ij}$  the maximum weight estimate obtained for seed  $i$  and mode  $j$ . Note that two body decay modes,  $\tau^- \rightarrow \pi^- \nu_\tau$  (3) and  $\tau^- \rightarrow K^- \nu_\tau$  (6), have no associated weight since the kinematics is fixed in these cases.

The impact of TAUOLA’s initialisation on physics results is investigated by considering  $10^6$  seed values, and by recording their corresponding  $W_{ij}$  values. The seeds are drawn from a uniform distribution. As a figure of merit, in table 2 we report the ratio of extreme  $W_{\max}$  estimates for mode  $j$ , defined as

$$r_j = \frac{\max(W_{ij})}{\min(W_{ij})}, \quad (24)$$

where the min and max run over all seeds.

Let us recall that TAUOLA applies a security factor of 1.2 to its  $W_{\max}$  estimate. Thus, assuming that  $\max(W_{ij})$  is indeed the upper bound,  $r_j \leq 1.2$  guarantees identical physics results for the  $10^6$  seed values, for mode  $j$ . In the present study, this condition is satisfied only for 7 out of 20 decay modes. Actually, for some modes, e.g. the 5<sup>th</sup> one corresponding to  $\tau \rightarrow a_1^- \nu_\tau$ , the maximum weight is likely not found out of  $10^6$  trials, since no convergence is observed.

Let us point out that this convergence issue could be observed already in the very first TAUOLA papers; see e.g. the “TEST RUN OUTPUT” appendix in Jadach et al. [1, 3] where the DADMAA routines reports a significant number of “overweighted” events.

Finding a single seed that would maximise the 20  $W_{\max}$  values simultaneously seems nearly impossible. Therefore, we use a more pragmatic approach in Alouette, as following. Let us write  $\overline{W}_j$  the median value for the estimate of  $W_{\max}$  for mode  $j$ . Among all tested seeds, we selected the one yielding estimates closest to  $\overline{W}_j$  according to least squares, i.e. the one minimising the L2-norm  $\|\mathbf{W} - \overline{\mathbf{W}}\|$ . When initialising TAUOLA, this “median” seed is used as default value by Alouette for its internal PRNG.

As a cross-check, we consider CM  $\tau^-$  decays, and we compare the distributions obtained for the resulting  $\nu_\tau$  energy,  $E_\nu$ , using the median seed and the respective “min”

Table 2: Ratios  $r_j$  of maximum to minimum  $W_{\max}$  estimates. The ratios have been computed from  $10^6$  initialisations using Alouette’s internal PRNG, with seed values drawn from a uniform distribution.

| Mode ( $j$ ) | ratio ( $r_j$ ) | Mode ( $j$ ) | ratio ( $r_j$ ) |
|--------------|-----------------|--------------|-----------------|
| 1            | 1.14            | 13           | 1.00            |
| 2            | 1.15            | 14           | 2.58            |
| 4            | 1.21            | 15           | 2.47            |
| 5            | 36.1            | 16           | 3.22            |
| 7            | 1.04            | 17           | 7.13            |
| 8            | 3.61            | 18           | 2.23            |
| 9            | 1.45            | 19           | 3.65            |
| 10           | 2.62            | 20           | 1.33            |
| 11           | 1.00            | 21           | 1.37            |
| 12           | 1.00            | 22           | 1.05            |

and “max” seeds for each decay mode. We compare  $E_\nu$  values since our concern with Alouette is  $\nu_\tau$ - $\tau$  transport. The comparison was performed with  $10^8$  Monte Carlo events per decay mode. As an example, figure 1 shows the results obtained for the 5<sup>th</sup> mode, the most pathological one according to table 2. It can be seen that the central parts of the  $E_\nu$  distributions are nearly identical using the median or the max seed. However, for the min seed a significant deviation is observed, with a 4 % maximum difference on the PDF. Similar results are observed for other modes. The bulk of the  $E_\nu$  distributions agree using the median or the max seed, within statistical uncertainties. But the min result can deviate significantly for some modes, i.e. for  $\tau^- \rightarrow a_1^- \nu_\tau$  (5),  $\tau^- \rightarrow \pi^0 K^- K^0 \nu_\tau$  (16) and  $\tau^- \rightarrow \pi^- \pi^0 K^0 \nu_\tau$  (19). Thus, for unlucky seed values erroneous physics results are obtained. Note also that our test does not allow to check if the PDF differ in tails, due to an insufficient number of events in these regions.

Given the previous results, using a median seed is a satisfactory solution for Alouette, whose main scope is  $\nu_\tau$ - $\tau$  transport. In addition, the median seed is efficient CPU wise. Indeed, the larger the estimate of  $W_{\max}$ , the larger the number of rejected samples when simulating a tentative decay. Note also that in any case the user can set its own seed value instead of the median one, if desired.

#### 4.2. Forward Monte Carlo

Forward Monte Carlo results are validated by comparison to Tauola++. Of particular interest for  $\nu_\tau$ - $\tau$  transport is the  $E_\nu$  spectrum of the daughter neutrino energy, as discussed previously. In order to validate the end-to-end forward procedure implemented in Alouette, let us now consider decays of a high energy, 1 TeV,  $\tau^-$  lepton instead of CM ones. A comparison of Alouette and Tauola++ results is shown on figure 2, for  $10^8$  Monte Carlo events. Three spin polarisation cases are considered for the  $\tau^-$ , right handed ( $P = +1$ ), unpolarised ( $P = 0$ ) and left handed ( $P = -1$ ). Alouette and Tauola++ agree within Monte Carlo statistical uncertainties. A similar agreement is also obtained when decaying  $\tau^+$  leptons instead of  $\tau^-$ .

When performing these comparisons, one should take care that Tauola++ uses a different convention than Alouette. Indeed, Tauola++ scope is to decay  $\tau^- \tau^+$  pairs

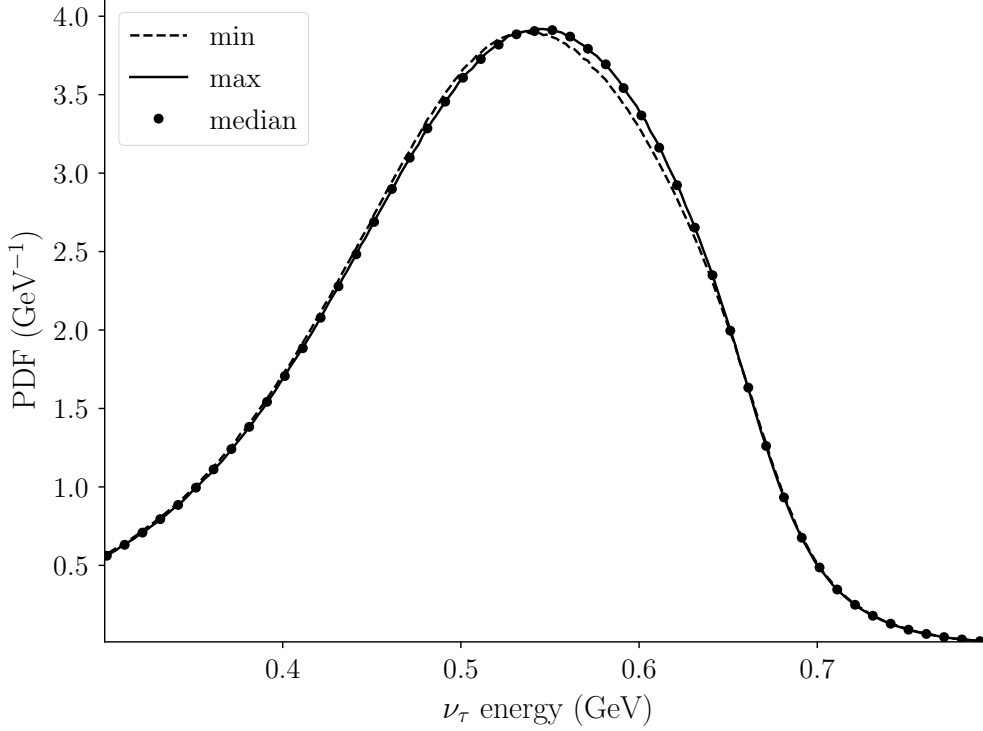


Figure 1: Comparison of  $\nu_\tau$  energy spectrums obtained with different PRNG seeds for TAUOLA’s initialisation. A CM  $\tau^- \rightarrow a_1^- \nu_\tau$  decay is considered, i.e. 5<sup>th</sup> mode, with a null spin polarisation. The solid (dashed) line corresponds to the seed yielding the maximum (minimum)  $W_{\text{max}}$  value, for the 5<sup>th</sup> mode. Dots correspond to the median seed, used by default in Alouette.

produced simultaneously. Thus, in Tauola++,  $\tau^-$  always propagate along the  $-z$  axis, while  $\tau^+$  along  $z$  (see e.g. section 4 of Davidson et al. [5]). As a result, a spin polarisation  $z$ -component of  $+1$  ( $-1$ ) should be given to the `Tauola::decayOne` method for a left (right) handed  $\tau^-$ . But opposite values should be used in the case of a  $\tau^+$  decay, which might be confusing. In comparison, Alouette lets the user explicitly specify momentum and spin polarisation for the mother particle as 3-vectors.

#### 4.3. Backward Monte Carlo

The validation of Alouette backward Monte Carlo results deserves a more detailed discussion, since BMC methods are usually less familiar than forward ones. Comparisons of forward and backward results are performed using toy experiments. Let us first describe the model used for these experiments, and then let us present the results of two test cases.

#### 4.3.1. Toy model

The following toy model is considered. Let us assume a primary flux of  $\tau$ -leptons,  $\Phi_0$ , with a fraction  $f_0$  of  $\tau^-$  and  $1 - f_0$  of  $\tau^+$ . Let  $\phi_0 = d\Phi_0/dp_0$  denote the differential flux w.r.t. the  $\tau$  momentum,  $p_0$ , and let us set  $\Phi_0 = 1$ . Thus,  $\phi_0$  is also the PDF of  $p_0$ . Let us further restrict values of  $p_0$  to an interval  $[p_{\min}, p_{\max}]$ . The toy experiment consist in decaying this primary flux of  $\tau$ -leptons, using Alouette, and then in recording the daughter particles whose momenta  $p_i$  also fall in  $[p_{\min}, p_{\max}]$ . Let  $\phi_i$  denote the corresponding differential flux and  $\Phi_i$  its integral.

Let us briefly recall the forward Monte Carlo computation of  $\Phi_i$  using a bias procedure. Let  $N$  denote the total number of Monte Carlo iterations and let us index them by  $k$ . For each Monte Carlo iteration, first a primary  $\tau$  is generated. The  $\tau$  charge value is drawn from a uniform distribution with a probability  $f_0$  for a  $\tau^-$ . The  $\tau$  momentum is generated using a  $1/p$  bias distribution, as

$$\ln p_{0,k} = \ln p_{\min} + \xi_k \ln \left( \frac{p_{\max}}{p_{\min}} \right), \quad (25)$$

where  $\xi_k$  is a random variate uniformly distributed over  $[0, 1]$ , drawn using Alouette PRNG. This bias procedure amounts to a uniform sampling in log scale, which is usually efficient for spectra spanning several orders of magnitude. Let us recall that sampling according to equation (25) corresponds to the following bias PDF

$$b(p_0) = \frac{1}{p_0 \ln \left( \frac{p_{\max}}{p_{\min}} \right)}. \quad (26)$$

Thus, forward Monte Carlo events are weighted by  $\omega_{b,F} = \phi_0(p_{0,k})/b(p_{0,k})$ .

Secondly, the  $\tau$  is decayed. Let us write  $m_{ik}$  the number of daughters particles of type  $i$  with final momenta in  $[p_{\min}, p_{\max}]$ . It follows that the forward Monte Carlo estimate of  $\Phi_i$  writes

$$\bar{\Phi}_{i,F} = \frac{1}{N} \sum_{k=1}^N \phi_{ik,F}, \quad (27)$$

$$\phi_{ik,F} = m_{ik} \frac{\phi_0(p_{0,k})}{b(p_{0,k})}. \quad (28)$$

Let us further recall that, owing to the Central Limit Theorem (CLT), the “Monte Carlo error”, i.e.  $\epsilon_i = \bar{\Phi}_{i,F} - \phi_i$ , converges to a Gaussian distribution for large  $N$ , as  $1/\sqrt{N}$ . An error estimate is given by the standard deviation of Monte Carlo samples, as

$$\bar{\sigma}_{i,F}^2 = \frac{1}{N-1} \left( \frac{1}{N} \sum_{k=1}^N \phi_{ik,F}^2 - \bar{\Phi}_{i,F}^2 \right). \quad (29)$$

Let us point out that the Monte Carlo computation needs to record only two quantities, the sum of weights  $\sum \phi_{ik,F}$  and the sum of squared weights  $\sum \phi_{ik,F}^2$ . From those, the Monte Carlo estimate and its corresponding uncertainty are derived, using equations (27) and (29).

The backward Monte Carlo computation of  $\Phi_i$  is similar to the forward one, but reverting the simulation flow. A bias procedure is used, applying corollary 4 of Niess et al. [22]. For each Monte Carlo event, first the final momentum  $p_{ik}$  of daughter  $i$  is drawn from a  $1/p$  bias distribution, using equation (25) but substituting  $p_{0,k}$  with  $p_{ik}$ . Secondly, the daughter particle is undecayed yielding the mother particle with charge  $C_k = \pm 1$  and momentum  $p_{0,k}$ . In addition, companion daughter particles are also produced by Alouette. The Monte Carlo weight due to this bias procedure is

$$\omega_{b,B} = \frac{f(C_k)\phi_0(p_{0,k})}{b(p_{ik})}, \quad (30)$$

where

$$f(C) = \begin{cases} f_0 & \text{if } C = -1, \\ 1 - f_0 & \text{otherwise.} \end{cases} \quad (31)$$

Thus,  $f\phi_0$  corresponds to the differential flux of  $\tau^-$  or of  $\tau^+$  particles, depending on the backward sampled mother particle.

As previously, let  $m_{ik}$  denote the number of daughters  $i$  with momenta in  $[p_{\min}, p_{\max}]$ , considering both the initial daughter and its decay companions. The total backward weight corresponding to this event is

$$\phi_{ik,B} = m_{ik} \frac{f(C_k)\phi_0(p_{0,k})}{b(p_{ik})} \omega_{B,k}, \quad (32)$$

where  $\omega_{B,k}$  is the BMC weight returned by Alouette, computed according to equation (23). Note that since the toy model flux is integrated using spherical coordinates, Alouette's undecay function must be configured accordingly. Thus, an additional factor  $p_{ik}^2/p_{0,k}^2$  is applied by Alouette to the Jacobian BMC weight given by equation (17), as detailed in 2.2.3.

The backward Monte Carlo estimate  $\bar{\Phi}_{i,B}$  of the flux  $\Phi_i$ , and its corresponding uncertainty  $\bar{\sigma}_{i,B}$ , are obtained from equations (27) and (29). We proceed as in the forward case, but substituting the weight  $\phi_{i,F}$  with the backward one,  $\phi_{i,B}$ .

There is an additional subtlety in the backward computation that we need to mention. If the multiplicity of a daughter is larger than one, then it is not correct to generate its final momentum over  $[p_{\min}, p_{\max}]$ , despite this is used as selection criteria. Instead, one should actually use  $[0, p_{\max}]$  as interval for the bias distribution. The reason is the following. When same type particles are produced, some of them might lie in  $[p_{\min}, p_{\max}]$  while others are below  $p_{\min}$ . Those are still valid events, nevertheless. In order to properly generate those events, one must consider that the backward sampled particle might have a momentum below  $p_{\min}$ , while its “twines” not necessarily. However, equation (25) does not allow to set a null lower bound. Thus, in practice we set the lower bound to a fraction  $\epsilon p_{\min}$  of  $p_{\min}$ , where  $\epsilon = 10^{-2}$ . I.e. the momentum  $p_{ik}$  is actually log-sampled over  $[\epsilon p_{\min}, p_{\max}]$ .

Obviously, the toy case considered herein does not illustrate the benefits of the backward Monte Carlo procedure. BMC appears similar, yet less straightforward than the usual forward computation. Backward methods are efficient for asymmetric problems. For example, BMC methods are good at sampling rare secondary events, in a narrow phase-space, from an extended primary flux. However, since in such cases forward computations are inefficient, comparisons would be difficult. Therefore, we instead consider

a symmetric toy model. This is a good stress-test for the backward procedure, since forward and backward methods have similar Monte Carlo efficiencies.

#### 4.3.2. Differential flux

As a first test, let us compare the differential fluxes obtained by backward and forward computations for a particular case. Let us consider a  $1/p^2$  primary flux composed of high energy left handed  $\tau^-$  and right handed  $\tau^+$  in equal fractions, i.e.  $f_0 = 1/2$ . Let us set  $p_{\min} = 100$  GeV and  $p_{\max} = 1$  PeV. The differential flux  $\phi_i$  is estimated by Monte Carlo using a log-uniform grid of momentum values. The procedure is similar to the one described previously for computing the total flux  $\Phi_i$ , using equations (27) and (29). But, the grid intervals are considered when computing the multiplicities  $m_{ik}$  instead of the total range  $[p_{\min}; p_{\max}]$ .

Figure 3 shows the results obtained with  $N = 10^7$  Monte Carlo events. The forward and backward Monte Carlo computations agree within statistical uncertainties. As an aside, this figure also provides a comparison of inclusive spectra of secondary particles in high energy  $\tau$  decays.

#### 4.3.3. Systematic tests

In addition, we performed systematic comparisons of the backward and forward results for the total flux  $\Phi_i$ . In order to test all cases separately, the primary flux is composed only of  $\tau^+$  or of  $\tau^-$ , i.e.  $f_0 = 0$  or 1. Three spin polarisations are considered in each case, left, right and unpolarised. A  $1/p$  primary spectrum is used with momenta between  $p_{\min} = 1$  GeV and  $p_{\max} = 1$  TeV. This allows us to cross-check the backward procedure for low relativistic boost ( $\gamma$ ) values as well. With these settings, we computed the total flux of secondary particles for all possible decay modes and sub-modes. We simulated  $N = 10^6$  Monte Carlo events per test case, resulting in relative accuracies on  $\Phi_i$  varying between 0.1 and 0.2 %.

Let  $\bar{\Phi}_{ij,F}$  ( $\bar{\Phi}_{ij,B}$ ) denote the total flux obtained for daughter  $i$  and decay mode  $j$  using the forward (backward) Monte Carlo computation. Let  $\bar{\sigma}_{ij,F}$  ( $\bar{\sigma}_{ij,B}$ ) be the corresponding error estimate. In order to assess the agreement between forward and backward computations we form the following test statistic

$$t_{ij} = \frac{\bar{\Phi}_{ij,F} - \bar{\Phi}_{ij,B}}{\sqrt{\bar{\sigma}_{ij,F}^2 + \bar{\sigma}_{ij,B}^2}}. \quad (33)$$

As null test hypothesis,  $\mathcal{H}_0$ , it is assumed that the forward (backward) Monte Carlo result is distributed as a Gaussian with expectation  $\Phi_{ij,0}$  and variance  $\sigma_{ij,F}^2$  ( $\sigma_{ij,B}^2$ ). Thus, we assume that the CLT limit is reached. Under  $\mathcal{H}_0$ ,  $t_{ij}$  follows a normal distribution. Therefore, let us call “significance” the values obtained for  $t_{ij}$ .

The significance values obtained for an unpolarised flux of  $\tau^-$  are shown on figure 3, as a test matrix. For this configuration, the worse significance value is  $2.8\sigma$  out of  $n = 141$  test cases. In order to assess if this is indeed significant, or not, the “look-elsewhere effect” must be accounted for. This is done by forming the following test statistic

$$T = \max(t_{ij}^2). \quad (34)$$

Under  $\mathcal{H}_0$ , the CDF of  $T$  is  $\left(F_{\chi_1^2}\right)^n$ , where  $F_{\chi_1^2}$  is the CDF of a  $\chi^2$  distribution with 1 degree of freedom. It follows that a worse significance  $t_{ij}$  of  $2.8\sigma$  corresponds to a look-elsewhere corrected  $p$ -value of 51.4%. Similar results are obtained when considering other polarisation values and / or a flux of  $\tau^+$  particles. Considering all test cases, we obtain a global  $p$ -value of 32.5% with a worse significance of  $-3.5\sigma$  out of 846 test cases. Thus, we conclude that we observe no significant differences between the forward and backward Monte Carlo results, with a relative accuracy of 0.1-0.2% on the total fluxes  $\Phi_i$ .

## 5. Conclusion

In the first part of this paper, section 2, we have presented a reverse Monte Carlo algorithm for simulating particle decays, i.e. algorithm 2. This algorithm allows one to invert a forward Monte Carlo engine using the Jacobian BMC method, introduced in Niess et al. [22]. The method only requires that the forward engine produces CM decays, preferentially with the possibility to specify the decay mode. Algorithm 2 has been applied to  $\tau$  decays with TAUOLA, which constitute a comprehensive use case. Thus, we consider this algorithm general enough to be transposable to other particle decays than  $\tau$  ones.

Section 2 is complementary to Niess et al. [22]. It illustrates the utility of the Jacobian BMC method for reverse Monte Carlo, since it provides a simple way to undecay Monte Carlo particles. In addition, section 2 emphasises the importance of coordinate systems when computing the Jacobian BMC weight, which has not been discussed previously.

In the second part of this paper, section 3, the Alouette library has been presented. The library is structured in three layers.

- (1) The first layer is a slightly modified version of TAUOLA Fortran (from Tauola++ 1.1.8 for LHC), refactored in order to comply to what we would expect from a library. The refactoring is done procedurally using a Python script. It does not modify any TAUOLA algorithm. It only relocates routines, redirects some critical calls, and it unifies external library symbols under the `tauola_` namespace using the Fortran 2003 `BIND(C)` attribute. This refactored TAUOLA is not intended for Alouette end-users. However, it could serve as a starting point for other C developers, sharing similar design concerns, and wishing to integrate TAUOLA Fortran in their own project.
- (2) The second layer is the Alouette C library. It implements the algorithms discussed in section 2. Alouette's API is intended to be simple when the library is used for transport problems, like  $\nu_\tau$ - $\tau$ . TAUOLA's initialisation is automated with robust settings, in particular for its "warmup", i.e. the determination of  $W_{\max}$  values. Thus, end-users need to call only a single library function, `alouette_decay` or its undecay version in BMC mode. In addition, the same PRNG is used in the C and Fortran layers, and it can be modified at runtime.
- (3) The third layer is a Python package wrapping the Alouette C library. As a result, the Python and C APIs are almost identical. The wrapping is done using `ctypes` and `numpy`. This allows us to expose Fortran and C data as familiar `numpy.ndarrays`. Binary distributions of Alouette are available from PyPI, for Linux and OSX.



In the third part of this paper, section 4, we presented the results of various validation tests of Alouette. In forward Monte Carlo mode, Alouette and Tauola++ results agree within Monte Carlo uncertainties, considering  $10^8$  events. Backward and forward Monte Carlo results are also found in agreement, with a relative accuracy of 0.1-0.2%.

Alouette has been implemented on top of Tauola++ “LHC” release. This release does not include the latest developments discussed in Chrzaszcz et al. [7]. The LHC release will be obsolete as TAUOLA physics is updated using latest developments (e.g. based on Belle II [38, 39] results). Thus, future improvements of Alouette should support recent TAUOLA releases as well, not only the LHC one.

## Acknowledgements

The author thanks an anonymous reviewer for its critical reading which contributed to improve the present paper. In addition, we gratefully acknowledge support from the CNRS/IN2P3 Computing Center (Lyon - France) for providing computing resources needed for this work. The analysis of Monte Carlo data has been done with numpy [35]. Validation figures have been produced using matplotlib [40] and a cmasher [41] colour map.

## Appendix A. Backward Monte Carlo weight

The backward Monte Carlo weight is given by the determinant of the Jacobian matrix corresponding to the change of variable between  $\mathbf{p}_0$ , the mother momentum, and  $\mathbf{p}_j$ , the daughter momentum. This change of variable is expressed by equation (13). Let us first compute the corresponding Jacobian matrix. A point of caution should be raised here. When deriving  $\mathbf{p}_0$  as function of  $\mathbf{p}_j$ ,  $\mathbf{p}_j^*$  should be considered as a constant, even in the polarised case where a bias CM decay process depending on  $\mathbf{p}_j$  is used. That is,  $L^{-1}$  should be differentiated only w.r.t. its first variable. This can be seen as  $L$  and  $L^{-1}$  are reciprocal only w.r.t. their first variable. In other words, the CM decay process is not inverted in the BMC procedure. It is biased though.

Using Cartesian coordinates, the Jacobian matrix can be expressed as

$$\frac{\partial \mathbf{p}_0}{\partial \mathbf{p}_j} = \frac{m_0}{d} \begin{bmatrix} a_x \Delta_x + b & a_x \Delta_y & a_x \Delta_z \\ a_y \Delta_x & a_y \Delta_y + b & a_y \Delta_z \\ a_z \Delta_x & a_z \Delta_y & a_z \Delta_z + b \end{bmatrix}, \quad (\text{A.1})$$

where

$$a_x = \frac{1}{E_j} \left[ p_{j,x} - (E_j + E_j^*) \frac{p_{j,x} E_j^* + E_j p_{j,x}^*}{d} \right], \quad (\text{A.2})$$

$$b = E_j + E_j^*, \quad (\text{A.3})$$

$$d = E_j E_j^* + \mathbf{p}_j \cdot \mathbf{p}_j^* + m_j^2, \quad (\text{A.4})$$

$$\Delta_x = p_{j,x} - p_{j,x}^*. \quad (\text{A.5})$$

The quantities  $a_y$ ,  $\Delta_y$ ,  $a_z$  and  $\Delta_z$  are obtained from  $a_x$  and  $\Delta_x$  by substituting  $x$  with  $y$  or  $z$ .

The determinant is conveniently computed using equation (A.1). Indeed, most terms simplify out. Only the factors in  $b^2$  and  $b^3$  remain. Thus

$$\left| \frac{\partial \mathbf{p}_0}{\partial \mathbf{p}_j} \right| = \frac{m_0^3}{d^3} [(a_x \Delta_x + a_y \Delta_y + a_z \Delta_z) b^2 + b^3]. \quad (\text{A.6})$$

Developing the previous results, after some manipulations one finds

$$\left| \frac{\partial \mathbf{p}_0}{\partial \mathbf{p}_j} \right| = \frac{m_0^3}{d^3} (E_j + E_j^*)^2 \frac{(E_j + E_j^*)^2 - d}{E_j}. \quad (\text{A.7})$$

Noting that  $\gamma + 1 = (E_j + E_j^*)^2/d$ , one can express the determinant as function of  $\gamma = E_0/m_0$ , which yields equation (17).

## References

- [1] S. Jadach, J. H. Kühn, Z. Was, Comput. Phys. Commun. 64 (1991) 275–299. [https://doi.org/10.1016/0010-4655\(91\)90038-M](https://doi.org/10.1016/0010-4655(91)90038-M).
- [2] M. Jezabek, Z. Was, S. Jadach, J. Kühn, Comput. Phys. Commun. 70 (1992) 69–76. [https://doi.org/10.1016/0010-4655\(92\)90092-D](https://doi.org/10.1016/0010-4655(92)90092-D).
- [3] S. Jadach, Z. Was, R. Decker, J. Kühn, Comput. Phys. Commun. 76 (1993) 361–380. [https://doi.org/10.1016/0010-4655\(93\)90061-G](https://doi.org/10.1016/0010-4655(93)90061-G).
- [4] P. Golonka, B. Kersevan, T. Pierzchała, et al., Comput. Phys. Commun. 174 (2006) 818–835. <https://doi.org/10.1016/j.cpc.2005.12.018>.
- [5] N. Davidson, G. Nanava, T. Przedzinski, et al., Comput. Phys. Commun. 183 (2012) 821–843. <https://doi.org/10.1016/j.cpc.2011.12.009>.
- [6] I. M. Nugent, T. Przedzinski, P. Roig, et al., Phys. Rev. D 88 (2013) 93012. <https://doi.org/10.1103/PhysRevD.88.093012>.
- [7] M. Chruszcz, T. Przedzinski, Z. Was, J. Zaremba, Comput. Phys. Commun. 232 (2018) 220–236. <https://doi.org/10.1016/j.cpc.2018.05.017>.
- [8] R. Abbasi, Y. Abdou, T. Abu-Zayyad, et al., Astropart. Phys. 35 (2012) 615–624. <https://doi.org/10.1016/j.astropartphys.2012.01.004>.
- [9] S. Adrian-Martinez, M. Ageron, F. Aharonian, et al., J. Phys. G: Nucl. Part. Phys. 43 (2016) 84001. <https://doi.org/10.1088/0954-3889/43/8/084001>.
- [10] I. Allekotte, A. Barbosa, P. Bauleo, et al., Nucl. Instrum. Methods Phys. Res., Sect. A 586 (2008) 409–420. <https://doi.org/10.1016/j.nima.2007.12.016>.
- [11] E. Bugaev, Astropart. Phys. 21 (2004) 491–509. <https://doi.org/10.1016/j.astropartphys.2004.03.002>.
- [12] O. B. Bigas, O. Deligny, K. Payet, V. V. Elewuyck, Phys. Rev. D 78 (2008) 63002. <https://doi.org/10.1103/PhysRevD.78.063002>.
- [13] J. Álvarez Muñoz, R. A. Batista, A. B. V, et al., Sci. China Phys. Mech. 63 (2020). <https://doi.org/10.1007/s11433-018-9385-7>.
- [14] J. Alvarez-Muñiz, W. R. Carvalho, K. Payet, et al., Phys. Rev. D 97 (2018) 023021. <https://doi.org/10.1103/PhysRevD.97.023021>.
- [15] J. Alvarez-Muñiz, W. R. Carvalho, A. L. Cummings, et al., Phys. Rev. D 99 (2019) 069902. <https://doi.org/10.1103/PhysRevD.99.069902>.
- [16] I. Safa, A. Pizzuto, C. A. Argüelles, et al., J. Cosmol. Astropart. Phys. 2020 (2020) 012–012. <https://doi.org/10.1088/1475-7516/2020/01/012>.
- [17] A. Garcia, R. Gauld, A. Heijboer, J. Rojo, J. Cosmol. Astropart. Phys. 2020 (2020) 025–025. <https://doi.org/10.1088/1475-7516/2020/09/025>.
- [18] V. Niess, O. Martineau-Huynh (2018). <https://doi.org/10.48550/arXiv.1810.01978>.
- [19] GitHub: niess/danton, 2022. <https://github.com/niess/danton>.
- [20] M. H. Kalos, Nucl. Sci. Eng. 33 (1968) 284–290. <https://doi.org/10.13182/NSE68-A19235>.
- [21] B. Eriksson, C. Johansson, M. Leimdorfer, M. H. Kalos, Nucl. Sci. Eng. 37 (1969) 410–422. <https://doi.org/10.13182/NSE69-A19116>.

- [22] V. Niess, A. Barnoud, C. Cârloganu, E. L. Ménédeu, *Comput. Phys. Commun.* 229 (2018) 54–67. <https://doi.org/10.1016/j.cpc.2018.04.001>.
- [23] V. Niess, *Comput. Phys. Commun.* 279 (2022) 108438. <https://doi.org/10.1016/j.cpc.2022.108438>.
- [24] GitHub: niess/pumas, 2022. <http://niess.github.io/pumas>.
- [25] GitHub: niess/ent, 2022. <https://github.com/niess/ent>.
- [26] S. Jadach, Z. Was, *Acta Phys. Pol. B* 15 (1984) 1151.
- [27] K. M. Graczyk, *Nucl. Phys. B Proc. Suppl.* 139 (2005) 150–153. <https://doi.org/10.1016/j.nuclphysbps.2004.11.230>.
- [28] GitHub: niess/alouette, 2022. <https://github.com/niess/alouette>.
- [29] RTD: alouette, 2022. <https://alouette.readthedocs.io/en/latest/>.
- [30] Tauola++ website, 2022. <https://tauolapp.web.cern.ch/tauolapp/>.
- [31] M. Fujikawa, H. Hayashii, S. Eidelman, et al., *Phys. Rev. D* 78 (2008) 72006. <https://doi.org/10.1103/PhysRevD.78.072006>.
- [32] M. Matsumoto, T. Nishimura, *ACM Trans. Model. Comput. Simul.* 8 (1998) 3–30. <https://doi.org/10.1145/272991.272995>.
- [33] P. A. Zyla, R. M. Barnett, J. Beringer, et al., *Prog. Theor. Exp. Phys.* 2020 (2020). <https://doi.org/10.1093/ptep/ptaa104>.
- [34] PyPI: cffi, 2022. <https://pypi.org/project/cffi/>.
- [35] C. R. Harris, K. J. Millman, S. J. van der Walt, et al., *Nature* 585 (2020) 357–362. <https://doi.org/10.1038/s41586-020-2649-2>.
- [36] PyPI: alouette, 2022. <https://pypi.org/project/alouette/>.
- [37] N. Nethercote, J. Seward, *ACM*, 2007, pp. 89–100. <https://doi.org/10.1145/1250734.1250746>.
- [38] E. Kou, P. Urquijo, W. Altmannshofer, et al., *Prog. Theor. Exp. Phys.* 2019 (2019). <https://doi.org/10.1093/ptep/ptz106>.
- [39] E. Kou, P. Urquijo, W. Altmannshofer, et al., *Prog. Theor. Exp. Phys.* 2020 (2020). <https://doi.org/10.1093/ptep/ptaa008>.
- [40] J. D. Hunter, *Comput. Sci. Eng.* 9 (2007) 90–95. <https://doi.org/10.1109/MCSE.2007.55>.
- [41] E. van der Velden, *J. Open Source Softw.* 5 (2020) 2004. <https://doi.org/10.21105/joss.02004>.

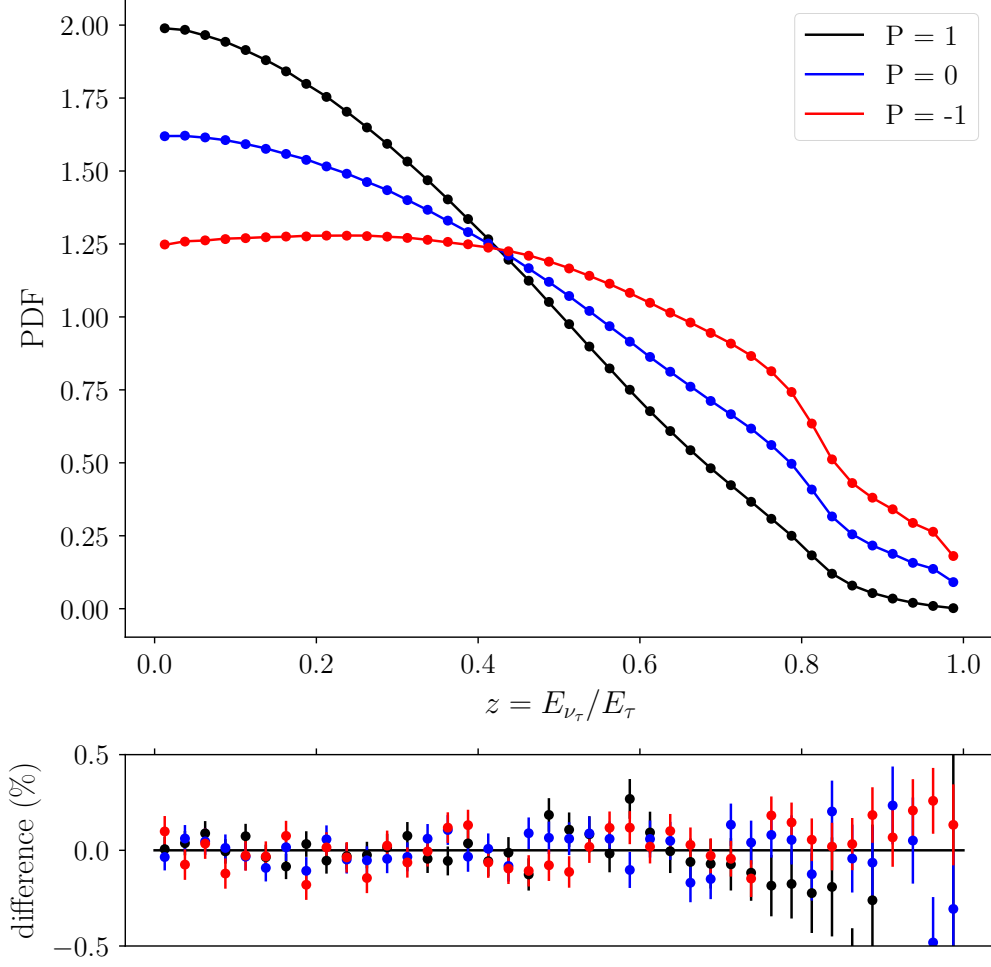


Figure 2:  $\nu_\tau$  energy spectra from the decay of 1 TeV  $\tau^-$  leptons. Three spin polarisation values are considered, as indicated in the legend. The solid lines stand for Alouette v1.0.1 results while dots are for Tauola++ v1.1.8 (LHC) [30]. The upper plot shows the absolute PDFs while the lower one indicates the relative differences between Alouette and Tauola++. Error bars correspond to Monte Carlo uncertainty estimates.

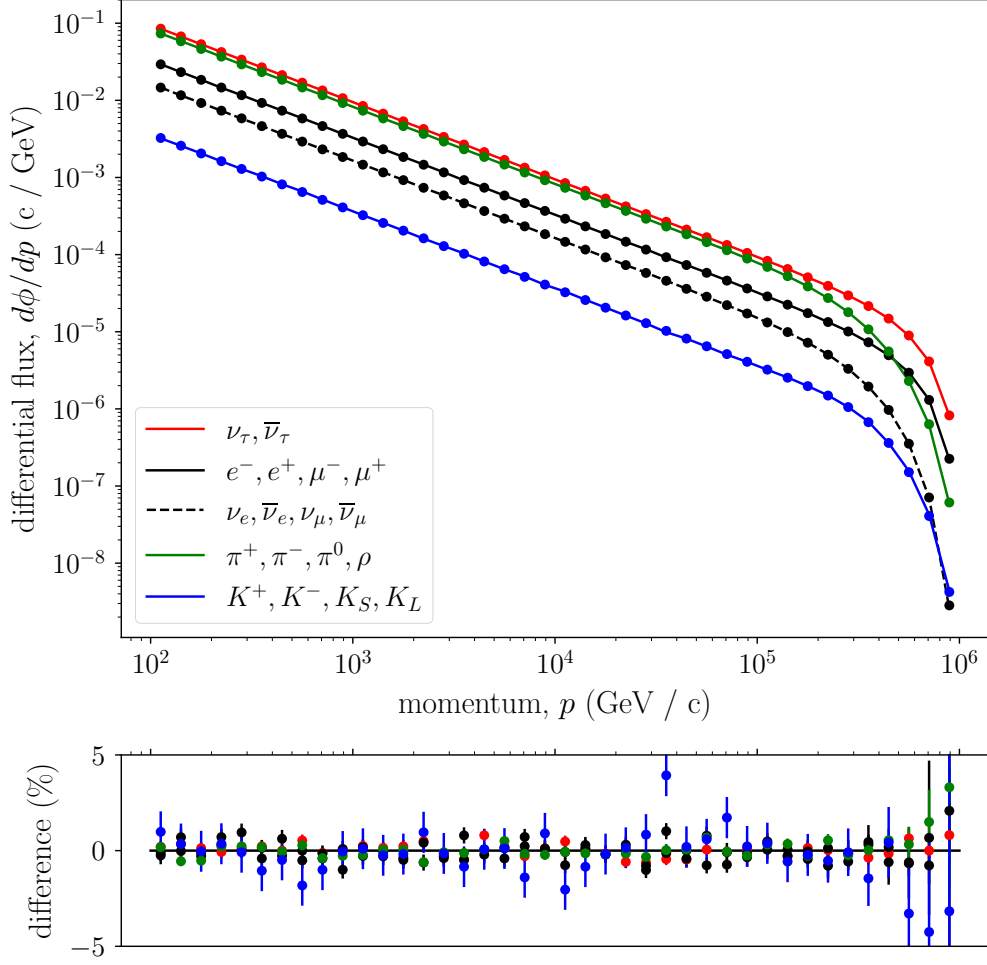


Figure 3: Spectrum of secondaries from the decay of a  $1/p^2$  flux of polarised  $\tau$ -leptons, with momentum between  $p_{\min} = 100 \text{ GeV}$  and  $p_{\max} = 1 \text{ PeV}$ . The solid lines stand for the backward Monte Carlo computation while dots indicate the results obtained with a forward Monte Carlo. Both computations have been carried out with Alouette v1.0.1. The upper plot shows the differential flux while the lower one is the relative difference between forward and backward computations. Error bars indicate Monte Carlo uncertainty estimates.

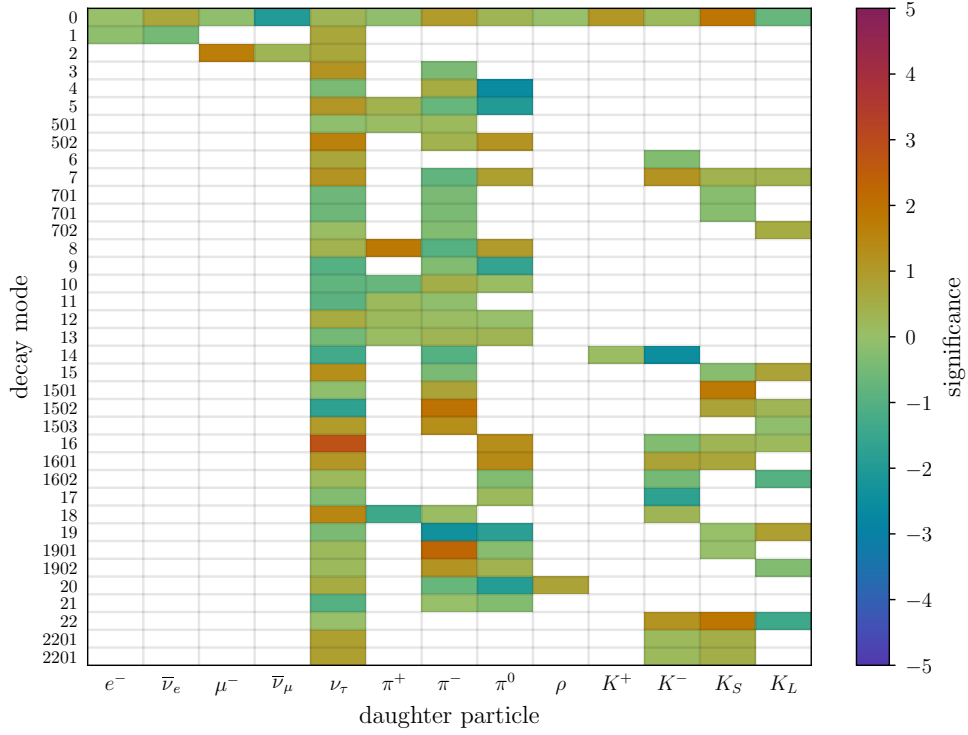


Figure 4: Test matrix for a unit flux of left handed  $\tau^-$  with momentum between  $p_{\min} = 1 \text{ GeV}$  and  $p_{\max} = 1 \text{ TeV}$ . The test compares forward and backward Monte Carlo computations of the total flux  $\Phi_i$  of daughter particles  $i$  from decays. All computations have been performed with Alouette v1.0.1. The significance of the difference is reported for different combinations of decay modes and daughter particles.